coatings

MDPI

Article

Ag Functionalization of Al-Doped ZnO Nanostructured Coatings on PLA Substrate for Antibacterial Applications

Daniele Valerini [1,*], Loredana Tammaro [2], Giovanni Vigliotta [3], Enrica Picariello [3], Francesco Banfi [4], Emanuele Cavaliere [5], Luca Ciambriello [5] and Luca Gavioli [5]

1 Laboratory of Functional Materials and Technologies for Sustainable Applications (SSPT-PROMAS-MATAS), ENEA—Italian National Agency for New Technologies, Energy and Sustainable Economic Development, S.S. 7 Appia, km 706, 72100 Brindisi, Italy
2 Nanomaterials and Devices Laboratory (SSPT-PROMAS-NANO), ENEA—Italian National Agency for New Technologies, Energy and Sustainable Economic Development, Piazzale E. Fermi, 1, Portici, 80055 Napoli, Italy; loredana.tammaro@enea.it
3 Department of Chemistry and Biology "A. Zambelli", University of Salerno, Via Giovanni Paolo II, 112, Fisciano, 80144 Salerno, Italy; gvigliotta@unisa.it (G.V.); enrica.picariello@hotmail.it (E.P.)
4 FemtoNanoOptics group, Université de Lyon, CNRS, Université Claude Bernard Lyon 1, Institut Lumière Matière, F-69622 Villeurbanne, France; francesco.banfi@univ-lyon1.fr
5 Interdisciplinary Laboratories for Advanced Materials Physics (i-LAMP) and Dipartimento di Matematica e Fisica, Università Cattolica del Sacro Cuore, Via Musei 41, 25121 Brescia, Italy; Emanuele.Cavaliere@unicatt.it (E.C.); luca.ciambriello@unicatt.it (L.C.); luca.gavioli@unicatt.it (L.G.)
* Correspondence: daniele.valerini@enea.it

Received: 20 November 2020; Accepted: 14 December 2020; Published: 17 December 2020

Abstract: Developing smart, environmentally friendly, and effective antibacterial surfaces is fundamental to contrast the diffusion of human infections and diseases for applications in the biomedical and food packaging sectors. To this purpose, here we combine aluminum-doped zinc oxide (AZO) and Ag to grow nanostructured composite coatings on bioplastic polylactide (PLA) substrates. The AZO layers are grown by RF magnetron sputtering, and then functionalized with Ag in atomic form by RF magnetron sputtering and in form of nanoparticles by supersonic cluster beam deposition. We compare the morphology, wettability, and antimicrobial performance of the nanostructured coatings obtained by the two methods. The different growth modes in the two techniques used for Ag functionalization are found to produce some differences in the surface morphology, which, however, do not induce significant differences in the wettability and antimicrobial response of the coatings. The antibacterial activity is investigated against *Escherichia coli* and *Staphylococcus aureus* as representatives of Gram-negative and Gram-positive bacteria, respectively. A preferential antimicrobial action of Ag on the first species and of AZO on the second one is evidenced. Through their combination, we obtain a hybrid composite coating taking advantage of the synergistic dual action of the two materials deposited, with a total bacterial suppression within few minutes for the first species and few hours for the second one, thus representing a valuable solution as a wide-spectrum bactericidal device.

Keywords: antimicrobial coatings; aluminum-doped zinc oxide (AZO); RF sputtering (RFS); supersonic cluster beam deposition (SCBD); silver nanoparticles; atomic force microscopy (AFM); health; biomedical applications; food packaging

1. Introduction

High-performance functional coatings represent one of the most effective strategy to confer antimicrobial properties to surfaces where avoiding human infections and disease diffusion are primary issues [1]. Such surfaces should be able to kill pathogen microorganisms or inhibit their growth and biofilm formation, as well as to prevent diffusion of foodborne diseases and reduce food degradation to preserve quality and increase shelf-life [2]. The use of antimicrobial surfaces can limit the cross-contamination phenomena due to the transfer of microorganisms from a contaminated surface to another. Moreover, due to the multiple simultaneous mechanisms of actions introduced by the coating materials, bacterial resistance is harder to be developed with respect to conventional antibiotics [3]. The development of efficient antibacterial materials is therefore a key aspect for a wide range of applications—such as biomedical devices (medical equipment, surgery tools, implants, etc.), food and beverage packaging materials, and textiles—just to mention a few. On the other hand, employed materials should also ensure environmental safety, no secondary toxicity to human health, or even biocompatibility, depending on the final use. To this aim, proper design of composition and structure of surface coatings turns out to be essential to achieve all the required properties. Apart from intrinsic biocide action of the coating material itself, other characteristics may be taken into account to enhance the antimicrobial efficacy, such as tuning of surface features (nanostructuration, roughness, etc.) and suitable combination of multiple active elements.

ZnO-based materials provide a strong bactericide action and physico-chemical stability, although the safety for human health is still debated in literature, especially for nanoparticles (NPs) [4,5]. Doping or combining ZnO with other elements can enhance its antimicrobial properties and favorably modify other characteristics like mechanical, optical, and gas/water vapor barrier properties. For example, Al-doped ZnO nanomaterials have been reported as effective antibacterial agents against different Gram-positive and Gram-negative species [6–8]. In the first report dealing with antimicrobial properties of AZO coatings [6], nanostructured Al-doped ZnO films were grown by sputtering a target source composed of mixed ZnO and Al_2O_3, since both components exhibit antibacterial properties [4,5] and, at the same time, they are both considered biocompatible and authorized as additives in food contact plastic materials [8]. Aiming to develop an environmentally friendly and health-safe composite, in our experiments the coatings were applied onto polylactide, a nature-derived polymer with several useful properties, biocompatible, bioresorbable, biodegradable and compostable [6,8]. In our previous works, such AZO coatings on PLA presented a polycrystalline phase composition, they demonstrated long-term stability (low release of material in physiological saline solution) and were shown to possess strong antibacterial action against different Gram-positive and Gram-negative species, without any significant toxicity detected on some human cell lines tested. To further improve the antimicrobial performance of those coatings, in the present work we add silver as supplementary material well-known for its antibacterial properties [9]. Both Ag and ZnO-based materials are identified to act against microbial species by means of several mechanisms, like release of active species (e.g., metal ions and reactive oxygen species ROS) or release of particles, with consequent cell membrane rupture, particle internalization inducing metabolic alterations, electrostatic interactions between the bacterial wall and the active materials and mechanical damaging of cell membrane and structure [4–9]. As a consequence, their arrangement into composite coatings can be expected to enhance the total antimicrobial action through the combined action of the two materials. In particular, herein two different methods are explored to functionalize the AZO surface with the Ag add-on: RF magnetron sputtering (RFS) and supersonic cluster beam deposition (SCBD). Differently from the sputtering deposition, where the depositing species are mainly constituted by atoms and ions, in the SCBD technique Ag NPs are already formed in the gas phase and then directed towards the substrate [10]. As a consequence, the diverse growth regimes occurring in the two methods may give rise to different surface morphologies of the Ag-functionalized AZO deposits on PLA. Atomic force microscopy, contact angle measurements and antibacterial tests are then conducted to investigate the differences in the properties of the mixed

coatings and to compare the responses of the single layer coatings (only AZO on PLA and only Ag on PLA) with those of the multicomponent hybrid layers (Ag-functionalized AZO coatings on PLA).

2. Materials and Methods

AZO coatings were deposited at room temperature by RF magnetron sputtering in a vacuum chamber (Sistec thin film equipment, Angelantoni Group, Italy) pumped down to a base pressure of 1×10^{-4} Pa. A ZnO:Al_2O_3 target (composition 98:2 wt.%, purity 99.999%, diameter 10 cm) was sputtered at RF power of 150 W in Ar + O_2 atmosphere at process pressure of 3 Pa, with relative flux percentage of 90% Ar and 10% O_2. Prior to the deposition, the cathode power was gradually increased until the set point of 150 W in about 30 min in the same Ar + O_2 atmosphere, and further cleaning and conditioning of the target surface was carried on for additional 10 min before to start the deposition process on the substrates. The coatings were simultaneously deposited on PLA films (extruded as previously reported [6]) and reference silicon substrates, passing under the sputtering target through rotation at 5 rpm for 20 min, resulting in AZO thickness of 30 nm, as measured by stylus profilometry.

The AZO layers were functionalized by depositing Ag under different growth regimes through the use of two different techniques: RF magnetron sputtering and supersonic cluster beam deposition. For the Ag-functionalization by means of RFS, a set of AZO samples was coated in the same equipment described above, by sputtering Ag at 50 W in Ar atmosphere, with the substrates passing under the target for a fixed number of 11 cycles at 5 rpm. Another set of samples was functionalized by SCBD at room temperature and at a base pressure of 1×10^{-4} Pa, following the same procedure described elsewhere [11–13], depositing Ag NPs on the sputter-deposited AZO films. In brief, SCBD relies on pulsed plasma ablation of a 99.99% purity Ag rod (ACI alloys), followed by NP condensation and expansion through a custom designed aerodynamic focusing system, directing the NPs to the substrate. The 6-nm thickness of the Ag layers was measured by atomic force microscopy on a silicon reference substrate deposited together with the PLA substrates. In addition to the Ag-functionalized AZO coatings (labeled as Ag/AZO), also single AZO and Ag coatings on PLA were deposited for comparison. For the discussion of the results, hereafter the samples deposited on PLA substrates will be labeled as AZO, Ag(RFS), Ag(SCBD), Ag(RFS)/AZO, and Ag(SCBD)/AZO, while the reference Ag samples deposited on silicon substrates will be labeled as Ag(RFS)/Si and Ag(SCBD)/Si, where the acronym 'RFS' or 'SCBD' in brackets stands for the technique used for the Ag deposition.

Atomic force microscopy data were obtained by an AFM (Park NX10, Park Systems, Suwon, Korea) in non-contact and tapping mode. PPP-NHCR tips (resonance frequency in the 250–280 kHz range, nominal tip radius 10 nm) were employed. The raw AFM data were analyzed with Gwyddion, extracting the grain size by a watershed algorithm.

Contact angles of ultrapure water and diiodomethane on coatings deposited on PLA substrates were measured by sessile drop method using an OCA 20 (Dataphysics, Filderstadt, Germany) goniometer, and data were collected with SCA 202 software (version 3.4.3 build 76). Equilibrium (static) contact angles were measured for 1 μL droplet volumes. Measurements were made on 10 different locations for each condition and the average value was reported with its standard deviation. To compute the surface free energy from measured contact angles the Owens, Wendt, Rabel, and Kaelble (OWRK) method [14] was applied and the related polar and dispersive components were evaluated by the Ström et al. equation [15], where the dispersion (non-polar) and polar components of the surface tension of the liquids employed were 21.8 and 51.0 mN/m for water and 50.8 and 0 mN/m for diiodomethane, respectively.

Effect of the different coated films on microorganism survival was evaluated as previously reported [8], with few variations. Briefly, *Escherichia coli* and *Staphylococcus aureus* were pre-inoculated aerobically for 12 h at 37 °C in Luria-Bertani (LB) medium (10 g·L^{-1} tryptone, 5 g·L^{-1} yeast extract, 10 g·L^{-1} NaCl), with constant shaking at 250 rpm. Bacteria were collected by centrifugation for 10 min at 3500 g, re-suspended at cellular density of 0.01 and 0.02 OD600 for *E. coli* and *S. aureus*, respectively (about 1 and 3×10^7 colony forming units, CFUs), in the presence of 1 cm^2 of sample (each cut into

four equal parts) and incubated at 37 °C under constant agitation at 50 rpm by vertical rotator. *E. coli* was re-suspended in sterile distilled water, while *S. aureus*, more sensitive to oligotrophic conditions was re-suspended in peptone water (1 g·L^{-1} peptone, 5 g·L^{-1} NaCl). A control with uncoated PLA was also inserted. At the times indicated 100 µl of each sample was suitably diluted, distributed on LB agar dishes (15 g·L^{-1} agar) and incubated for 18–24 h at 37 °C. Subsequently, the number of CFU/mL was quantified for each sample and the survival kinetics was determined as the percentage variation over time of CFUs with respect to the initial time t = 0. The values were plotted on a semilogarithmic scale as the mean ± standard deviation of three independent tests. The obtained CFUs were also used to calculate the antibacterial activity (*A*) [16]. For this purpose, the following formula was applied: $A = F - G$, where *F* represents the growth values in the presence of uncoated PLA, while *G* corresponds to the growth values with the coated samples. They are calculated according to the formula $F = (\text{Log } C_t - \text{Log } C_{t0})$ and $G = (\text{Log } T_t - \text{Log } T_{t0})$. *C* and *T* are CFUs detected for uncoated PLA control and coated samples, respectively, at different times up to 8 h. The PLA films were considered 'antimicrobial' when achieving an *A* greater than 2 (reduction in bacteria number >99%). Values were reported as the mean ± standard deviation of three independent analyses. The significance of the differences in the antimicrobial activity among the various treatments was evaluated by two-way ANOVAs (analyses of variance), followed by Tukey post hoc tests (for $\alpha = 0.05$).

3. Results and Discussion

3.1. Atomic Force Microscopy (AFM) Analyses

Three dimensional (3D) representation of the AFM data results of the AZO samples functionalized with Ag by the two different techniques, presented in Figure 1a,c, clearly show the presence of some wrinkling effects of the sample surface, corresponding to a rms roughness of 35 nm deriving from the AZO deposition on PLA. This rms value is in line with that one previously measured on AZO samples deposited at high RF power on PLA and ascribed to wrinkling effects induced on the polymer surface by the particle bombardment during the AZO sputtering deposition, as extensively described in our previous work [8]. To obtain the nanoscale grain size distribution it has been necessary to remove such wrinkling effect by a polynomial regression, and the resulting 3D images are reported in Figure 1b,d for Ag(RFS)/AZO and Ag(SCBD)/AZO, respectively.

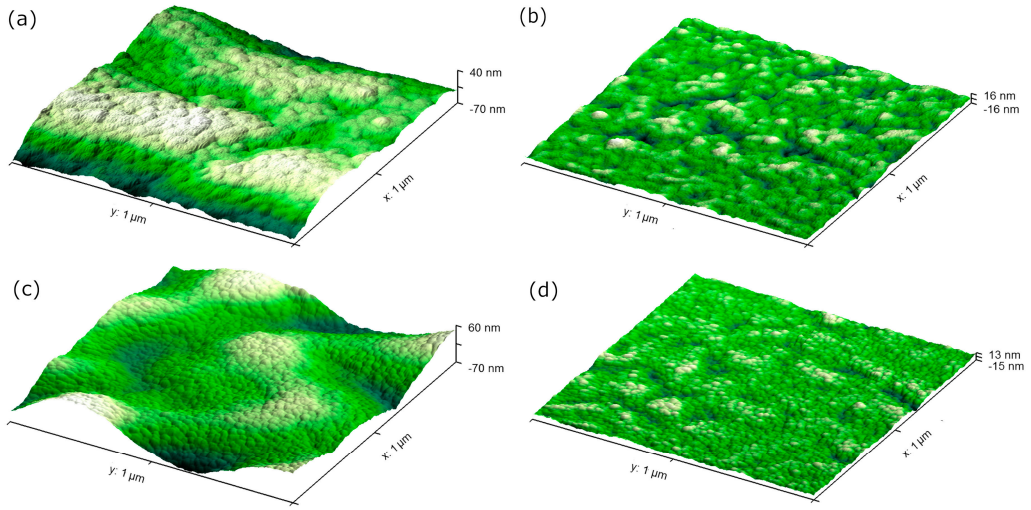

Figure 1. 3D AFM images of Ag/AZO coatings on PLA before (left) and after (right) fine correction: (**a**) and (**b**) Ag(RFS)/AZO; (**c**) and (**d**) Ag(SCBD)/AZO. For all images, the X:Y:Z scale ratio is 1:1:1.

After removing the background, the resulting AFM images of samples deposited on PLA substrates are shown in Figure 2 and the related rms roughness values are listed in Table 1.

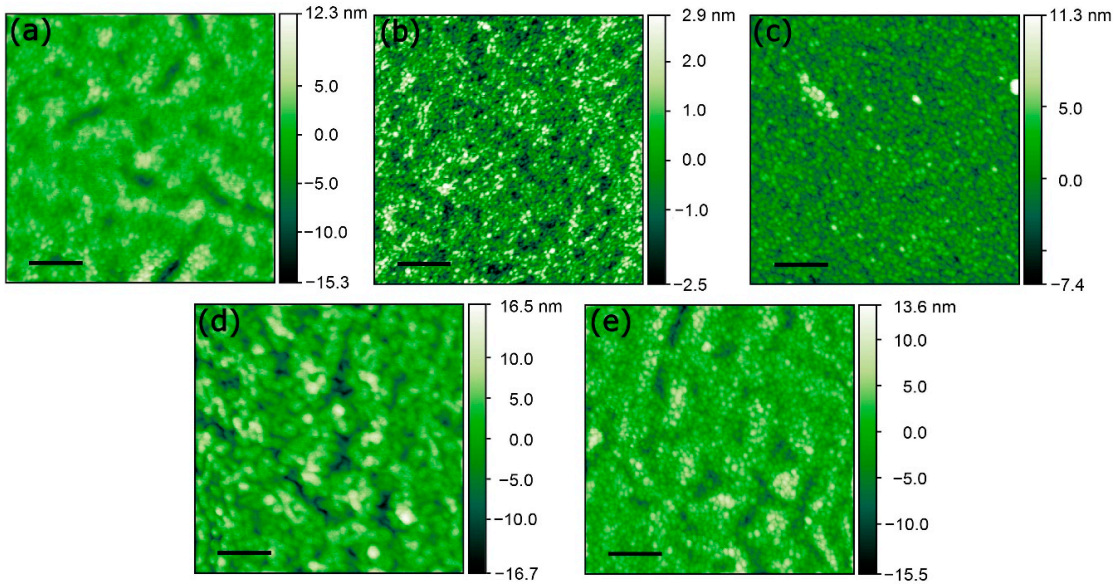

Figure 2. (1 × 1) μm^2 AFM images of films deposited on PLA: (**a**) AZO; (**b**) Ag(RFS); (**c**) Ag(SCDB); (**d**) Ag(RFS)/AZO; (**e**) Ag(SCBD)/AZO. Scale bar for all panels is 200 nm. Images in panels (**a**,**d**,**e**) have been subtracted a polynomial background to remove the roughness of the AZO/PLA layer.

Table 1. Rms roughness, height (mode of the distribution), and width (standard deviation) of height distributions obtained from the AFM analyses for coatings deposited on PLA and for reference Ag samples deposited on silicon.

Sample	Rms Roughness (±0.1 nm)	Height (±0.2 nm)	Distribution Width (±0.1 nm)
AZO	2.4	1.8	1.6
Ag(RFS)	0.9	1.2	1.1
Ag(SCBD)	1.9	2.2	1.9
Ag(RFS)/AZO	4.2	5.0	3.9
Ag(SCBD)/AZO	3.3	3.7	2.5
Ag(RFS)/Si	3.6	4.3	4.4
Ag(SCBD)/Si	1.1	1.2	1.4

The fine morphology appears to be constituted by nanometric clusters uniformly distributed over the sample surface and close one each other. In such samples, quantification of the NP size distribution from the projected surface area is affected by convolution effects of the tip. We hence obtain the grain size by measuring the height difference between the center of each grain and the height at the grain border, assuming that we are observing the top half of a NP with a spherical shape. Figure 3 displays the radius distribution of the different samples, that has been fitted with either Gaussian or lognormal distribution functions depending on the sample type. The RFS-synthesized samples are fitted with a Gaussian distribution reflecting the growth mode of the grains in an atom-by-atom mode. The SCBD-synthesized samples have been fitted with a lognormal distribution, since these layers are obtained by depositing directly NPs and not atoms, and hence reflect the typical size distribution of clusters produced by supersonic beams also for different materials [13,17–21]. The values of mode and width obtained from the fit of the height distributions are reported in Table 1.

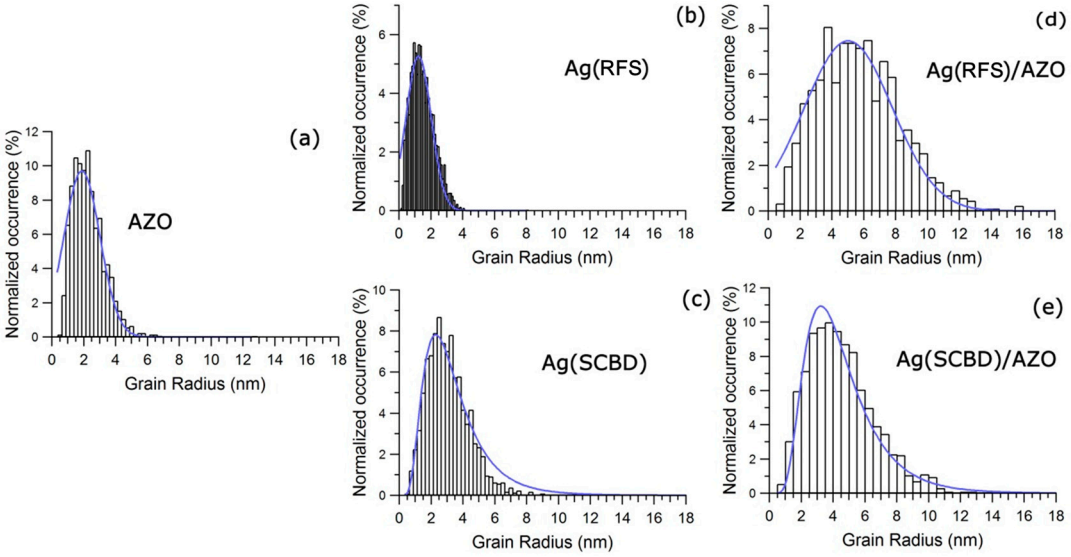

Figure 3. Nanoparticle height distributions obtained from the analysis of AFM data for samples deposited on PLA substrate: (**a**) AZO; (**b**) Ag(RFS); (**c**) Ag(SCDB); (**d**) Ag(RFS)/AZO; (**e**) Ag(SCBD)/AZO. The blue curves represent the best fit functions as described in the discussion.

The different growth mode of the Ag layers obtained from the two synthesis methods can be noticed already from the AFM images of samples directly deposited on PLA, shown in Figure 2b for Ag(RFS) and Figure 2c for Ag(SCBD) respectively, and from the striking difference of the related size distributions reported in Figure 3b,c. On the bare PLA, the mode of the Ag grain size is 1.2 ± 0.2 nm for the Ag(RFS) sample and 2.2 ± 0.2 nm for the Ag(SCBD) sample (see Table 1). On the AZO/PLA substrate the mode of the size distribution is 5.0 ± 0.2 nm for Ag deposited by RFS and 3.7 ± 0.2 nm for Ag deposited by SCBD. It is worth noting that for Ag deposited on reference silicon substrates (distributions not shown in Figure 3 for clarity, but fit values reported in Table 1), the mode of the distribution is 4.3 ± 0.2 nm for the Ag(RFS) and 1.2 ± 0.2 nm for the Ag(SCBD) sample. This behavior can be ascribed to the constituents produced by the two synthesis methods (mainly atoms and ions in RF sputtering, NPs in SCBD), to the substrate diffusion coefficient and to the kinetic energy of the atoms or NPs. The species synthesized by SCBD have an average energy of 0.1–0.5 eV/atom [21,22], while those produced by RF sputtering process have an energy of ~10 eV/atom [23,24], two orders of magnitude higher. On a silicon substrate, that is crystalline and with a rms lower than 0.2 nm, the landing energy of the RF sputtered atoms account for a large atomic diffusion over the surface, promoting the atoms coalescence into 4.3 ± 0.2 nm clusters. This behavior is almost absent for the less energetic SCBD NPs, which maintains their integrity upon landing, thus resulting in a mode of 1.2 ± 0.2 nm. On PLA, the atoms and the NPs may stick on the polymer surface or be easily implanted underneath the surface, thus hindering their mobility and blocking their coalescence into bigger clusters. This results in an almost four times reduction of the distribution mode (down to 1.2 ± 0.2 nm) for the Ag(RFS) deposit on PLA with respect to Si, while it is only slightly increasing the distribution mode (2.2 ± 0.2 nm) for the Ag(SCBD) sample. The single AZO coating on PLA forms grains of 1.8 ± 0.2 nm and presents a rms of 2.4 ± 0.1 nm, while these values increase in both the Ag-functionalized samples, as expected due to the superimposition of the Ag particles with the underlying AZO grains. In particular, the size distribution mode in the Ag(SCBD)/AZO sample increases to 3.7 ± 0.2 nm, mainly due to such cluster superimposition, since the NPs deposited by this method are not modified upon landing, as mentioned above. Differently, the observed grain size on the Ag(RFS)/AZO present a further increase, up to 5.0 ± 0.2 nm, indicating again a high mobility of Ag adatoms on the AZO surface and their consequent coalescence. To summarize, the combination of the synthesis methods (RF sputtering and SCBD) with the substrate role (adatom mobility and surface roughness) is providing a very good playground to modify the deposited grain size and final roughness of the Ag/AZO coatings.

3.2. Wettability Analyses

Contact angles measured for water and diiodomethane and related surface energies of the different coatings deposited on PLA are reported in Table 2 and plotted in Figure 4.

Table 2. Contact angles of water and diiodomethane and surface energy values for coatings deposited on PLA.

Sample	Contact Angle (°)		Surface Energy (mJ/m^2)		
	Water	Diiodomethane	Polar Component	Dispersion Component	Total
AZO	63.6 ± 3.2	55.8 ± 3.0	13.9	31.0	44.9 ± 2.7
Ag(RFS)	80.8 ± 2.3	49.6 ± 2.8	4.3	34.5	38.8 ± 1.8
Ag(SCBD)	91.8 ± 5.5	55.2 ± 2.4	1.6	31.3	32.9 ± 1.9
Ag(RFS)/AZO	93.7 ± 1.9	57.8 ± 3.9	1.4	29.9	31.3 ± 2.3
Ag(SCBD)/AZO	91.3 ± 5.9	55.9 ± 4.1	1.8	30.9	32.7 ± 2.8

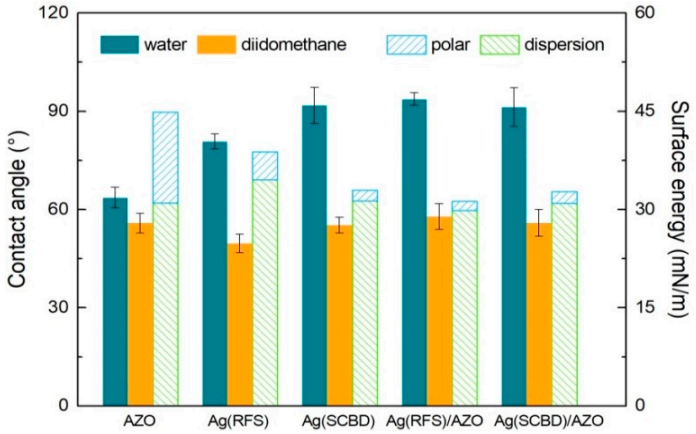

Figure 4. Contact angles (plain bars) and surface energy components (patterned bars) of samples deposited on PLA.

The water contact angle (WCA) values indicate that the water wettability of all the Ag-containing samples is significantly different from that one of the AZO coating, with the latter presenting a WCA of about 64° while the others showing higher WCAs around 80° or slightly above 90°. As a consequence of the Ag addition onto the AZO coating (samples Ag(RFS)/AZO and Ag(SCBD)/AZO), the surface behavior is then turned from moderately hydrophilic to slightly hydrophobic, regardless of the deposition technique used for the Ag functionalization. On the contrary, no particular variation is observed on the wettability with the non-polar solvent diiodomethane, where contact angles values are very similar for all the different coatings. In line with the differences in WCA, the total surface energy of the AZO layer is also different from that one obtained on samples having silver on their surface: the Ag presence on the surface reduces the total surface energy, where this decrease is primarily led by the strong reduction of the polar component (corresponding to the increase of the related contact angle with the polar liquid water).

Since the wettability of a surface is determined by a combination of its physico-chemical characteristics, one of the reasons for the WCA differences between the Ag-containing coatings and the unfunctionalized AZO sample can be related to the different chemical state of the surface (dangling bonds, terminal facets of the particles, oxidation, etc.) due to the presence of the Ag clusters. At the same time, influence of surface morphology can be deduced as well. Indeed, the lower contact angles observed for both water and diiodomethane in sample Ag(RFS) as compared to Ag(SCBD) can be attributed to its lower roughness, since the spread of a liquid droplet on a smooth surface is facilitated with respect to a rougher surface where air can be trapped below the droplet and hinder

its spread. On the contrary, the contact angle values obtained on sample Ag(RFS)/AZO increase to values comparable to the analogous sample Ag(SCBD)/AZO, due to the increased roughness when Ag is sputtered on the AZO coating, as described above.

3.3. Antimicrobial Tests

Results of antimicrobial tests performed on the Gram-negative bacterium *E. coli* and Gram-positive bacterium *S. aureus* are shown in Figure 5, reporting the bacterial survival rate at different time intervals for the various coated samples, together with the reference data of the control sample (i.e., uncoated PLA substrate). In order to quantify the net antimicrobial action of the coatings with respect to the control, the antimicrobial activity A of the coated samples was calculated as

$$A = F - G = \log \frac{C_t / C_{t0}}{T_t / T_{t0}} \quad (1)$$

with $F = (\text{Log } C_t - \text{Log } C_{t0})$ and $G = (\text{Log } T_t - \text{Log } T_{t0})$, where C_t and T_t are the CFUs detected at the different considered times t for control substrate and coated samples, respectively, and C_{t0} and T_{t0} are the respective CFUs at the initial time $t = 0$. The antimicrobial activity, whose values are listed in Table 3 and plotted in Figure 6, can be considered good when $A \geq 2$, and excellent when $A \geq 3$.

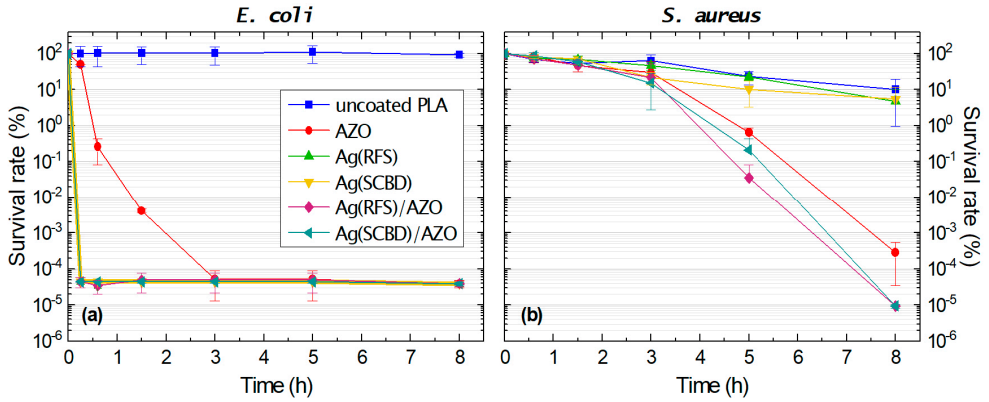

Figure 5. Antibacterial effect of the different samples against (**a**) the Gram-negative bacterium *E. coli* and (**b**) the Gram-positive bacterium *S. aureus*, at different time intervals. The survival rate is intended as the percentage reduction of CFU/mL with respect to $t = 0$. The y axes are in logarithmic scale.

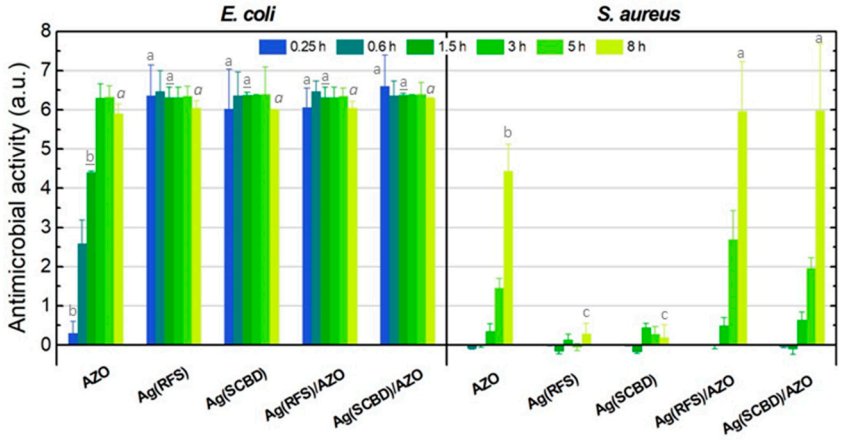

Figure 6. Antimicrobial activity (A) of the different samples against *E. coli* (left) and *S. aureus* (right). Statistical analysis refers at same times and, for each of them, different letters indicate significant differences among coated films ($p < 0.001$). The same character (normal, italic and underscored) is used for each considered time.

Table 3. Antimicrobial activity *A* against *E. coli* and *S. aureus*, calculated by Equation (1) at different times for samples deposited on PLA. Data are reported as the mean ± standard deviation.

Bacterial Species	Sample	Antimicrobial Activity (*A*)					
		Treatment Time (h)					
		0.25 *	**0.6**	**1.5**	**3**	**5**	**8**
E. coli	AZO	0.30 ± 0.30	2.59 ± 0.60	4.40 ± 0.04	6.30 ± 0.36	6.33 ± 0.28	5.90 ± 0.25
	Ag(RFS)	6.36 ± 0.78	6.47 ± 0.53	6.32 ± 0.26	6.32 ± 0.26	6.40 ± 0.25	6.00 ± 0.18
	Ag(SCBD)	6.03 ± 1.00	6.36 ± 0.60	6.37 ± 0.08	6.37 ± 0.02	6.40 ± 0.70	6.08 ± 0.01
	Ag(RFS)/AZO	6.06 ± 0.50	6.47 ± 0.27	6.32 ± 0.26	6.32 ± 0.26	6.35 ± 0.20	6.05 ± 0.17
	Ag(SCBD)/AZO	6.60 ± 0.80	6.36 ± 0.38	6.37 ± 0.05	6.37 ± 0.02	6.40 ± 0.30	6.30 ± 0.01
S. aureus	AZO	n.d.	−0.08 ± 0.03	0.02 ± 0.08	0.35 ± 0.19	1.45 ± 0.25	4.44 ± 0.69
	Ag(RFS)	n.d.	0.00 ± 0.03	−0.15 ± 0.08	0.13 ± 0.15	−0.05 ± 0.09	0.29 ± 0.26
	Ag(SCBD)	n.d.	0.00 ± 0.02	−0.17 ± 0.04	0.45 ± 0.10	0.28 ± 0.19	0.19 ± 0.33
	Ag(RFS)/AZO	n.d.	0.02 ± 0.02	0.00 ± 0.10	0.49 ± 0.21	2.70 ± 0.73	5.96 ± 1.27
	Ag(SCBD)/AZO	n.d.	−0.04 ± 0.03	−0.10 ± 0.14	0.64 ± 0.20	1.96 ± 0.26	5.98 ± 1.70

* Data at 0.25 h for *S. aureus* were not determined (n.d.) as there was no detectable variation with respect to $t = 0$.

The survival kinetics measured for *E. coli* (Figure 5a) demonstrate a strong bactericidal action of the unfunctionalized AZO coating, with a survival rate reaching the minimum detection limit (~3–5 CFU/mL) after about 3 h, corresponding to a reduction of cellular density higher than 6 Log ($A = 6.3$, i.e., reduction in bacterial population >99.9999 %), that is in line with results reported in our previous work on similar AZO samples [8]. However, the coatings made of only silver on PLA (Ag(RFS) and Ag(SCBD)) clearly evidence even far better behavior against *E. coli*, with an extremely fast action inducing the same reduction of about 6 Log in only 15 min. Then, the composite samples made of Ag-functionalized AZO coatings (Ag(RFS)/AZO and Ag(SCBD)/AZO) follow the same trend of the single Ag coatings (the survival rate curves of the Ag/AZO coatings and those of the Ag coatings are overlapped in Figure 5), indicating that, in the examined time range (minimum of 15 min), their antibacterial response is driven by the activity of silver.

In contrast, an opposite behavior is observed in the kinetics recorded for the Gram-positive bacterium *S. aureus* (Figure 5b), where the simple silver coatings demonstrate a very low antibacterial efficacy, while the response of the composite AZO + Ag coatings is mainly driven by the AZO contribution. As a preliminary observation, a weak antimicrobial influence on *S. aureus* can be detected at long time for the bare PLA substrate (uncoated control sample) too, inducing about 1 Log reduction of the bacterial colony counts after 8 h. This minimal effect can be probably ascribed to a rather low biocide action caused by the coarseness of the PLA surface, inducing mechanical detrimental effects (e.g., cell deformations and wall abrasion), and to environmental stress induced by the oligotrophic conditions of the incubation medium used during the microbiological tests. For longer exposition times either or both the factors could then result in a slight bacterial reduction. Such behavior is not observed on *E. coli* in the examined time range because, as a microbiological indicator of water quality, it is more stable in environments poor in organic substances compared to a pathogenic bacterium such as *S. aureus* [25,26].

Analyzing the results of the coated samples, the antibacterial action against *S. aureus* is shown to be slower than *E. coli* for all the films, as clearly evidenced in Figures 5 and 6. In particular, the activity *A* of the single AZO coating on *S. aureus* is moderate ($A < 2$) up to about 5 h, increasing to a value around 4.4 at 8 h, whereas on *E. coli* the same activity level of $A = 4.4$ is obtained after only 1.5 h and the coating exhibits a complete bactericidal action ($A > 6$) at 3 h. Generally, Gram-positive species like *S. aureus* are considered to have higher susceptibility to ZnO than Gram-negative ones like *E. coli*, due to the differences in thickness, complexity, and composition of cell membranes in the two families, as well as difference in their intracellular content, thus inducing different sensitivity to active species such as metal ions and reactive oxygen species [27]. However, it should be noted that, differently from *E. coli*, *S. aureus* tends to form multicellular aggregates that take longer to be destroyed, therefore high

bacterial suppression can be reached after longer exposure times with the active material, as shown in our previous work [8], thus explaining the slower biocidal effect observed on *S. aureus* at short periods.

Contrarily to what observed on *E. coli*, the single Ag coatings on PLA (Ag(RFS) and Ag(SCBD)) demonstrate a very low antimicrobial effect on *S. aureus* even at long times, with a response that is comparable to the bare PLA substrate, resulting in activity values *A* as low as ~0.2–0.3 at 8 h. The limited efficacy of Ag against *S. aureus* in comparison to *E. coli* observed in our experiments is in line with previous findings [11,28,29], and it was related to the different electrostatic interaction with the charged cell walls of the two bacterial species.

Concerning the composite coatings made of Ag-functionalized AZO layers, the trend of survival rate for *S. aureus* is found to be similar to that one of the single AZO coating, with a moderate improvement introduced by the silver presence. To our knowledge, there is no other report in literature about the antimicrobial properties of Ag-functionalized AZO coatings, thus we can only draw a general comparison with analogous materials made of combination of Ag with ZnO. The antibacterial behavior in our samples is similar or appears to be even faster, especially for *E. coli*, when compared to other kinds of Ag-modified ZnO nanomaterials (see e.g., [30–32] and references therein), observing the different activity of the two individual materials on Gram-negative and Gram-positive species and the beneficial effects of joining them together. In particular, in [31], Ag was shown to be less effective on *S. aureus* than *E. coli*, and the inhibitory effect was enhanced in the Ag/ZnO heterostructure NPs against both species, presenting a better response against the latter, which is in line with the behavior demonstrated by our samples too. Anyhow, it must be underlined that these properties are strongly dependent on a series of experimental factors, such as materials composition and concentration, form (different kinds of nanostructures), crystal structure, substrates, synthesis procedures, methodologies and parameters used for the antimicrobial tests, etc., thus making it impossible to definitely derive a reliable comparison. Our Ag/AZO coatings are able to reach a complete suppression of *E. coli* in only 15 min, while almost complete bactericide action against *S. aureus* is induced in about 8 h (around 6 Log of CFU reduction). This suppression rate for *S. aureus* in the hybrid coatings corresponds to an activity value that is about 1.3 times higher than the single AZO coating at the same exposure time. Considering the minor antibacterial action revealed for the individual Ag coatings against *S. aureus* as described above, the improvement observed for this bacterial species in the composite coatings can be only partially ascribed to the secondary additional contribution of silver on AZO. As a further enhancing factor, the increased surface roughness in the AZO + Ag coatings with respect to the single AZO film might also play a significant role in increasing the antimicrobial efficacy. Indeed, higher surface roughness has been reported as a key factor to increase the bactericidal action [8,33], in consequence of the enlarged effective contact area between the rough surface and the surrounding environment, promoting microbial adhesion through electrostatic interactions with the surface, and resultant enhanced bactericidal effects such as structural deformation of the microorganisms, abrasive damage of cell membranes, and fostered transfer of active species (metal ions and ROS) from the coating surface to the bacterial cells.

For both bacterial species here considered, no significant difference in the antimicrobial characteristics can be evidenced when comparing analogous samples where silver has been deposited by the two different techniques (RFS or SCBD). The bacterial suppression rate and related antimicrobial activities appear the same regardless of the process used for the Ag deposition in the two sets of samples, pointing out no substantial influence of the used deposition technique on the antimicrobial performance under the experimental conditions and time range here used. More complex experimental analyses should be needed in order to discern for possible fine differences in the antimicrobial response of these samples, especially in the case of *E. coli* where the drop of CFU counts is extremely rapid.

As an overall consideration, the Ag-functionalized AZO coatings on PLA here developed are shown to possess an excellent antibacterial activity against both considered microbial species, with an extremely rapid complete suppression of *E. coli* in a few minutes and a complete suppression of *S. aureus* in a few hours. Thanks to the preferential action of each material against one species or another (predominant efficacy of Ag on *E. coli* and of AZO on *S. aureus* in our samples) it is then

possible to obtain a composite coating exploiting the combined performance of both materials together, therefore being capable to simultaneously and efficiently strike both kinds of bacteria.

4. Conclusions

Ecofriendly antibacterial films made of Ag-functionalized Al-doped ZnO nanostructured coatings deposited on bioplastic PLA films were developed with the aim to find new solutions to contrast the diffusion of infections and diseases. Ag-functionalization was evaluated by two different deposition methods—RF sputtering and supersonic cluster beam deposition—as a way to tune the surface features (roughness and particle size) of the final Ag/AZO composite materials. Surface wettability was turned from moderately hydrophilic to slightly hydrophobic by the addition of Ag onto the AZO layer, together with some influence of surface roughness. The antimicrobial action of the Ag-functionalized AZO coatings to the Gram-negative *E. coli* was shown to be led by the Ag presence, while the response against the Gram-positive *S. aureus* was mainly driven by the AZO material. The combination of these materials together enhanced the biocide action, leading to an extremely fast total suppression of *E. coli* within few minutes, while *S. aureus* required some hours, due to the dissimilar bacterial walls and consequent interactions of the two species with the active materials, as well as to different tendency to form multicellular aggregates.

Thanks to the preferential bactericide action of Ag and AZO on the different bacterial species, the hybrid Ag/AZO coatings here developed are then able to exploit a synergistic action, providing simultaneous superior antimicrobial performance against both species with respect to the individual material deposits. They can therefore represent a promising solution to provide broader spectrum of action against different kinds of bacteria for different possible applications, like in food packaging and biomedical sectors. In perspective of these final applications, further insights in the evaluation of the active species releasing properties of these composite coatings can be required to get a deeper understanding of the mechanisms of action in damaging the cytoplasmic membrane of the bacterial cells and a correct evaluation of possible toxicity concerns for human cells.

Author Contributions: Conceptualization, D.V. and L.G.; Methodology, D.V., L.T., G.V., E.P., F.B., E.C., and L.G.; Investigation, all authors; Writing—original draft preparation, D.V. and L.G.; Writing—review and editing, all authors. All authors have read and agreed to the published version of the manuscript.

Funding: This work was supported by MIUR-FARB 2018–2019 funding from Università di Salerno (G.V., E.P.). L.G., E.C., L.C. acknowledge that this research was partially funded by Università Cattolica del Sacro Cuore through D.2.2 and D.3.1 grants.

Conflicts of Interest: The authors declare no conflict of interest.

References

1. Wille, I.; Mayr, A.; Kreidl, P.; Bruhwasser, C.; Hinterberger, G.; Fritz, A.; Posch, W.; Fuchs, S.; Obwegeser, A.; Orth-Holler, D.; et al. Cross-sectional point prevalence survey to study the environmental contamination of nosocomial pathogens in intensive care units under real-life conditions. *J. Hosp. Infect.* **2018**, *98*, 90–95. [CrossRef] [PubMed]
2. Wei, T.; Tang, Z.; Yu, Q.; Chen, H. Smart antibacterial surfaces with switchable bacteria-killing and bacteria-releasing capabilities. *ACS Appl. Mater. Interfaces* **2017**, *9*, 37511–37523. [CrossRef] [PubMed]
3. Wang, L.; Hu, C.; Shao, L. The antimicrobial activity of nanoparticles: Present situation and prospects for the future. *Int. J. Nanomed.* **2017**, *12*, 1227–1249. [CrossRef] [PubMed]
4. Kim, I.; Viswanathan, K.; Kasi, G.; Thanakkasaranee, S.; Sadeghi, K.; Seo, J. ZnO nanostructures in active antibacterial food packaging: Preparation methods, antimicrobial mechanisms, safety issues, future prospects, and challenges. *Food Rev. Int.* **2020**. [CrossRef]
5. Makvandi, P.; Wang, C.; Zare, E.; Borzacchiello, A.; Niu, L.; Tay, F. Metal-based nanomaterials in biomedical applications: Antimicrobial activity and cytotoxicity aspects. *Adv. Funct. Mater.* **2020**, *30*, 1910021. [CrossRef]

6. Valerini, D.; Tammaro, L.; Di Benedetto, F.; Vigliotta, G.; Capodieci, L.; Terzi, R.; Rizzo, A. Aluminum-doped zinc oxide coatings on polylactic acid films for antimicrobial food packaging. *Thin Solid Film.* **2018**, *645*, 187–192. [CrossRef]
7. Saxena, V.; Chandra, P.; Pandey, L. Design and characterization of novel Al-doped ZnO nanoassembly as an effective nanoantibiotic. *Appl. Nanosci.* **2018**, *8*, 1925–1941. [CrossRef]
8. Valerini, D.; Tammaro, L.; Villani, F.; Rizzo, A.; Caputo, I.; Paolella, G.; Vigliotta, G. Antibacterial Al-doped ZnO coatings on PLA films. *J. Mater. Sci.* **2020**, *55*, 4830–4847. [CrossRef]
9. Huang, J.; Li, X.; Zhou, W. Safety assessment of nanocomposite for food packaging application. *Trends Food Sci. Technol.* **2015**, *45*, 187–199. [CrossRef]
10. Wegner, K.; Piseri, P.; Tafreshi, H.; Milani, P. Cluster beam deposition: A tool for nanoscale science and technology. *J. Phys. D Appl. Phys.* **2006**, *39*, R439–R459. [CrossRef]
11. Cavaliere, E.; De Cesari, S.; Landini, G.; Riccobono, E.; Pallecchi, L.; Rossolini, G.; Gavioli, L. Highly bactericidal Ag nanoparticle films obtained by cluster beam deposition. *Nanomed.-Nanotechnol. Biol. Med.* **2015**, *11*, 1417–1423. [CrossRef] [PubMed]
12. Cavaliere, E.; Benetti, G.; Van Bael, M.; Winckelmans, N.; Bals, S.; Gavioli, L. Exploring the optical and morphological properties of Ag and Ag/TiO_2 nanocomposites grown by supersonic cluster beam deposition. *Nanomaterials* **2017**, *7*, 442. [CrossRef] [PubMed]
13. Benetti, G.; Cavaliere, E.; Banfi, F.; Gavioli, L. Antimicrobial nanostructured coatings: A gas phase deposition and magnetron sputtering perspective. *Materials* **2020**, *13*, 784. [CrossRef] [PubMed]
14. Owens, D.K.; Wendt, R.C. Estimation of the surface free energy of polymers. *J. Appl. Polym. Sci.* **1969**, *13*, 1741–1747. [CrossRef]
15. Ström, G.; Fredriksson, M.; Stenius, P. Contact angles, work of adhesion, and interfacial tensions at a dissolving hydrocarbon surface. *J. Colloid Interface Sci.* **1987**, *119*, 352–361. [CrossRef]
16. Pantani, R.; Gorrasi, G.; Vigliotta, G.; Murariu, M.; Dubois, P. PLA-ZnO nanocomposite films: Water vapor barrier properties and specific end-use characteristics. *Eur. Polym. J.* **2013**, *49*, 3471–3482. [CrossRef]
17. Milani, P.; Iannotta, S. *Cluster Beam Synthesis of Nanostructured Materials*, 1st ed.; Springer: Berlin/Heidelberg, Germany, 1999.
18. Barborini, E.; Kholmanov, I.; Piseri, P.; Ducati, C.; Bottani, C.; Milani, P. Engineering the nanocrystalline structure of TiO_2 films by aerodynamically filtered cluster deposition. *Appl. Phys. Lett.* **2002**, *81*, 3052–3054. [CrossRef]
19. Benetti, G.; Cavaliere, E.; Brescia, R.; Salassi, S.; Ferrando, R.; Vantomme, A.; Pallecchi, L.; Pollini, S.; Boncompagni, S.; Fortuni, B.; et al. Tailored Ag-Cu-Mg multielemental nanoparticles for wide-spectrum antibacterial coating. *Nanoscale* **2019**, *11*, 1626–1635. [CrossRef]
20. Benetti, G.; Cavaliere, E.; Canteri, A.; Landini, G.; Rossolini, G.; Pallecchi, L.; Chiodi, M.; Van Bael, M.; Winckelmans, N.; Bals, S.; et al. Direct synthesis of antimicrobial coatings based on tailored bi-elemental nanoparticles. *APL Mater.* **2017**, *5*, 036105. [CrossRef]
21. Benetti, G.; Caddeo, C.; Melis, C.; Ferrini, G.; Giannetti, C.; Winckelmans, N.; Bals, S.; Van Bael, M.; Cavaliere, E.; Gavioli, L.; et al. Bottom-up mechanical nanometrology of granular ag nanoparticles thin films. *J. Phys. Chem. C* **2017**, *121*, 22434–22441. [CrossRef]
22. Benetti, G.; Gandolfi, M.; Van Bael, M.; Gavioli, L.; Giannetti, C.; Caddeo, C.; Banfi, F. Photoacoustic sensing of trapped fluids in nanoporous thin films: Device engineering and sensing scheme. *ACS Appl. Mater. Interfaces* **2018**, *10*, 27947–27954. [CrossRef] [PubMed]
23. Depla, D.; Mahieu, S.; Greene, J.E. Chapter 5—Sputter Deposition Processes. In *Handbook of Deposition Technologies for Films and Coatings*, 3rd ed.; Martin, P.M., Ed.; William Andrew Publishing: Boston, MA, USA, 2010; pp. 253–296.
24. Maréchal, N.; Quesnel, E.; Pauleau, Y. Silver thin films deposited by magnetron sputtering. *Thin Solid Film.* **1994**, *241*, 34–38. [CrossRef]
25. Flint, K.P. The long-term survival of *Escherichia coli* in river water. *J. Appl. Bacteriol.* **1987**, *63*, 261–270. [CrossRef] [PubMed]
26. Watson, S.; Clements, M.; Foster, S. Characterization of the starvation-survival response of *Staphylococcus aureus*. *J. Bacteriol.* **1998**, *180*, 1750–1758. [CrossRef]
27. Gold, K.; Slay, B.; Knackstedt, M.; Gaharwar, A. Antimicrobial activity of metal and metal-oxide based nanoparticles. *Adv. Ther.* **2018**, *1*, 1700033. [CrossRef]

28. Kim, J.; Kuk, E.; Yu, K.; Kim, J.; Park, S.; Lee, H.; Kim, S.; Park, Y.; Park, Y.; Hwang, C.; et al. Antimicrobial effects of silver nanoparticles. *Nanomed.-Nanotechnol. Biol. Med.* **2007**, *3*, 95–101. [CrossRef]
29. Mendez-Pfeiffer, P.; Urzua, L.; Sanchez-Mora, E.; Gonzalez, A.; Romo-Herrera, J.; Arciniega, J.; Morales, L. Damage on *Escherichia coli* and *Staphylococcus aureus* using white light photoactivation of Au and Ag nanoparticles. *J. Appl. Phys.* **2019**, *125*, 213102. [CrossRef]
30. Lu, W.; Liu, G.; Gao, S.; Xing, S.; Wang, J. Tyrosine-assisted preparation of Ag/ZnO nanocomposites with enhanced photocatalytic performance and synergistic antibacterial activities. *Nanotechnology* **2008**, *19*, 445711. [CrossRef]
31. Zhang, Y.; Gao, X.; Zhi, L.; Liu, X.; Jiang, W.; Sun, Y.; Yang, J. The synergetic antibacterial activity of Ag islands on ZnO (Ag/ZnO) heterostructure nanoparticles and its mode of action. *J. Inorg. Biochem.* **2014**, *130*, 74–83. [CrossRef]
32. Agnihotri, S.; Bajaj, G.; Mukherji, S. Arginine-assisted immobilization of silver nanoparticles on ZnO nanorods: An enhanced and reusable antibacterial substrate without human cell cytotoxicity. *Nanoscale* **2015**, *7*, 7415–7429. [CrossRef]
33. Cao, F.; Zhang, L.; Wang, H.; You, Y.; Wang, Y.; Gao, N.; Ren, J.; Qu, X. Defect-rich adhesive nanozymes as efficient antibiotics for enhanced bacterial inhibition. *Angew. Chem.-Int. Ed.* **2019**, *58*, 16236–16242. [CrossRef] [PubMed]